PCCP

PAPER

View Article Online
View Journal | View Issue

Cite this: *Phys. Chem. Chem. Phys.*, 2014, **16**, 9876

Unraveling non-covalent interactions within flexible biomolecules: from electron density topology to gas phase spectroscopy

R. Chaudret,[a] B. de Courcy,*[a] J. Contreras-García,[a] E. Gloaguen,[bc] A. Zehnacker-Rentien,*[d] M. Mons*[bc] and J.-P. Piquemal*[a]

Received 2nd July 2013,
Accepted 6th October 2013

DOI: 10.1039/c3cp52774c

www.rsc.org/pccp

The NCI (Non-Covalent Interactions) method, a recently-developed theoretical strategy to visualize weak non-covalent interactions from the topological analysis of the electron density and of its reduced gradient, is applied in the present paper to document intra- and inter-molecular interactions in flexible molecules and systems of biological interest in combination with IR spectroscopy. We first describe the conditions of application of the NCI method to the specific case of intramolecular interactions. Then we apply it to a series of stable conformations of isolated molecules as an interpretative technique to decipher the different physical interactions at play in these systems. Examples are chosen among neutral molecular systems exhibiting a large diversity of interactions, for which an extensive spectroscopic characterization under gas-phase isolation conditions has been obtained using state-of-the-art conformer-specific experimental techniques. The interactions presently documented range from weak intra-molecular H-bonds in simple amino-alcohols, to more complex patterns, with interactions of various strengths in model peptides, as well as in chiral bimolecular systems, where invaluable hints for the understanding of chiral recognition are revealed. We also provide a detailed technical appendix, which discusses the choices of cut-offs as well as the applicability of the NCI analysis to specific constrained systems, where local effects require attention. Finally, the NCI technique provides IR spectroscopists with an elegant visualization of the interactions that potentially impact their vibrational probes, namely the OH and NH stretching motions. This contribution illustrates the power and the conditions of use of the NCI technique, with the aim of providing an easy tool for all chemists, experimentalists and theoreticians, for the visualization and characterization of the interactions shaping complex molecular systems.

1. Introduction

Non-covalent interactions play a fundamental role in determining and maintaining the three-dimensional structure of macromolecules involved in life chemistry and biology.[1] They are widely responsible for the secondary and tertiary structures of proteins, for the structure of DNA, and for subtle molecular recognition phenomena. Among them, conventional hydrogen bonds like those binding together the two strands of DNA can be described in terms of intermolecular interactions of medium to large strength. More subtle and difficult to describe are the intra-molecular hydrogen bonds, those of weaker strength like the CH$\cdots\pi$, OH or NH$\cdots\pi$, or CH$\cdots$O interactions, as well as dispersion between aromatic residues. Despite being weaker than conventional hydrogen bonds, these interactions play a major stabilizing role.[2,3] In this context, experimental gas-phase isolation of biomolecules and of their non-covalent complexes provides a unique tool for studying non-covalent interactions in the absence of solvent perturbations.[4,5] Moreover, when applied to model systems of medium size, these techniques coupled to spectroscopic methods allow direct comparison with quantum chemical or semi-empirical calculations. The systems studied so far range from simple neutral systems[6–18] to neutral,[16,17,19–25] cationised, or protonated polypeptides[25–28] providing convenient isolated models for conventional or unconventional hydrogen bonds.[2,29]

Coupled to quantum chemistry, gas-phase spectroscopy is able to take advantage of the sensitivity of the OH or NH stretch frequency to the local environment in order to determine efficiently the structures observed in the gas phase. Such conformation-selective IR spectroscopy studies allow experimentalists to explore

[a] *Sorbonne Universités, UPMC, Laboratoire de Chimie Théorique and CNRS, UMR 7616, 75252 Paris Cedex 05, Paris, France. E-mail: courcy@lct.jussieu.fr, jpp@lct.jussieu.fr*
[b] *CNRS, INP, Laboratoire Francis Perrin, URA 2453, 91191 Gif-sur-Yvette, France*
[c] *CEA, IRAMIS, Service des Photons, Atomes et Molécules, Laboratoire Francis Perrin, URA 2453, 91191 Gif-sur-Yvette, France. E-mail: michel.mons@cea.fr*
[d] *CNRS, Institut des Sciences Moléculaires d'Orsay (ISMO), UMR8214, and Univ. Paris-Sud, F-91405, Orsay, France. E-mail: anne.zehnacker-rentien@u-psud.fr*

the conformational preference of various flexible molecules. Several studies devoted to peptides have shown that the most prominent secondary structures of proteins, such as turns (γ-, β-, 3–10 helices, β-strands, β-hairpins, *etc.*...), can be observed under jet-cooled isolated conditions.[17–24,30–36] Such studies have illustrated how sensitive the structure is to the balance between the several interactions present and how even a weak one (like a NH···π interaction) is able to perform a fine tuning between different types of secondary structures.[21,37–40]

In the same context, a change of chirality of a residue within one peptide chain, or of one of the complexation partners within a complex of chiral molecules, results in a structural change, which is easily evidenced from spectroscopy.[22,41–48] The nature of the change ranges from subtle differences in dispersion forces between the homochiral and heterochiral complexes[49,50] to a drastic rearrangement of the binding pattern (OH···O *vs.* OH···N interaction, or hydrogen bond *vs.* dispersion).[51–53] In many cases, the difference between two diastereomeric interacting pairs rests on delicate interactions like CH···π or CH···O interactions, which are much weaker than the main interactions ensuring the stability of the complex.[54] These exemplary observations, as well as the other experimental works cited above, point to the need for novel user-friendly tools for the description of non-covalent interactions, especially the weak ones.

Quantum chemistry offers various strategies ranging from Density Functional Theory to post Hartree–Fock methods to energetically optimize structures and determine their vibrational signatures. Nevertheless, direct use of such computational results to address the chemical concepts of bonds and interactions in complex molecules requires an *a posteriori* interpretative treatment of the electronic density. Quantum Chemistry Topological methods[55–58] (QCT) have been widely used for this purpose, for example, to characterize intermolecular hydrogen bonds. Analysis of the electronic density as the chosen scalar function, namely the Quantum-Theory-of-Atoms-In-Molecules (QTAIM) approach,[59,60] relies on the properties of density critical points, where the gradient of the electron density cancels.[61] These critical points are characterized by the number of non-zero eigenvalues λ_1, λ_2, λ_3 of the Hessian matrix and the sum of the signs of the eigenvalues. Of special interest are the first order saddle points, so-called bond critical points (BCP), which are a signature of chemical bonds (including H-bonds). However, for weak intramolecular interactions, BCPs are not always found in the QTAIM context.[62a] It is therefore useful to resort to alternative topology-based methods[63,64] for characterizing such interactions.

In this contribution we propose to use a recently-introduced alternative interpretative technique, the Non-Covalent Interaction (NCI) approach, to unravel the different interactions at play in flexible molecules ranging from peptides to chiral systems. This method, which is also based on the analysis of the electron density,[64] enables us to identify and visualize the interactions that perturb the N–H or OH groups of these molecules of biological interest and control their vibrational spectroscopy. For example, NCI was recently shown[62b] to provide a regional definition of H-bond interactions that overcomes the shortcomings of only analyzing electron density critical points[62a,b] and generalized the bond critical point approach by extending it to the topology of the region surrounding it.[62b] And this can be done at a very low calculation cost.

NCI will be applied to a large sample of molecules encompassing various intra- and inter-molecular types of weak non-bonding interactions. The criterion for including a given system in the probed sample is the existence of recent and precise experimental spectroscopic data in the gas phase, leading to unambiguous structural assignment. We shall first describe simple paradigmatic examples where NCI enables disentangling the diverse intramolecular non-bonding interactions at play in model systems. We shall then apply this method to polypeptides in the gas phase, chosen to illustrate the large variety of interactions observed in these molecules. Last, we shall show that NCI can also be used for intermolecular interactions, like those involved in the emblematic example of chiral recognition.

2. Principle of the NCI approach

The NCI technique rests on the analysis and the graphical interpretation of the electronic density (ρ) and its derivatives, namely the λ_2 eigenvalue of its Hessian and its reduced gradient $s(\rho)$,[63,64] defined as:

$$s = \frac{1}{2(3\pi^2)^{1/3}} \frac{|\nabla\rho|}{\rho^{4/3}}$$

From a practical point of view, the procedure focuses on regions far from the nuclei, where weak inter- and intramolecular interactions manifest themselves through singularities of the electron density.[63,64] These singularities are related to the fact that electronic clouds located on interacting groups perturb each other, influencing the local densities and associated properties.

More specifically, NCI consists in analysing the domains of weak electron density and low reduced density gradient $s(\rho)$.

The NCI method rests essentially on the visualization of those loci of the space where the reduced gradient $s(\rho)$ is *close to zero*.

Whereas QTAIM focuses on the density critical points where the density gradient vanishes (*e.g.* at the BCPs), NCI generalizes the concept and focuses on loci where the reduced density gradient is low, *i.e.*, regions of space around these points. Emphasis is put on surfaces of space on which the reduced gradient takes a defined value, chosen to be close to zero. These reduced gradient isosurfaces, which are hereafter referred to as NCI isosurfaces or 3D-NCI plots, are also characterized by well-defined density values, since the gradient remains small along each of them.

NCI isosurfaces actually surround the QTAIM critical points when they exist. The interest of the NCI isosurfaces, however, is to remain defined even when no BCP is found, which enables an analysis of all types of intramolecular interactions, including those missed within the QTAIM framework.[63]

In order to consider weak interactions, both ρ and s must be weak by definition,[64] and therefore NCI should be used with

care in situations of high electron density, in particular when two atoms come very close to each other (covalent bonding, intramolecular interactions...). A precise discussion of the limits of validity of the method is given in the Technical appendix.

Moreover, NCI isosurfaces appear not only in the case of stabilizing interactions but also in the case of repulsive clashes (steric repulsion). In order to distinguish these interactions, NCI resorts to the local topology of the electron density, namely the curvatures of the density, λ_i, mentioned above. While the greatest and positive curvature, λ_1, is dictated by the interatomic line, the next largest eigenvalue λ_2 can vary in sign depending on the situation: it will be negative in bonding situations (like at BCPs) and positive in most of the non-bonding repulsive cases (see Technical appendix). Thus, the sign of the second eigenvalue, λ_2, is used to distinguish between these two extreme cases.

This information is used in so-called 2D NCI plots, which consist in plotting the reduced gradient (s) as a function of the electron density, ρ, oriented by the sign of λ_2. In the presence of close contacts between atoms, the behaviour of the reduced gradient remarkably differs from that in the atomic tails, by adopting vanishing values of $s(\rho)$ at these close contacts between atoms, and leading to troughs in the 2D NCI plots (see Fig. 1).[63,64] These troughs, especially the ρ value at the troughs, are the basis of the NCI approach. The 2D NCI-plots are then used as inputs to construct so-called 3D NCI plots, consisting in isosurfaces of the reduced gradient of the density enabling the spatial visualization of the close contacts.

NCI is then able to localize the non-covalent interactions between atoms, and label them as stabilizing or destabilizing according to the topology of the electronic density. The underlying

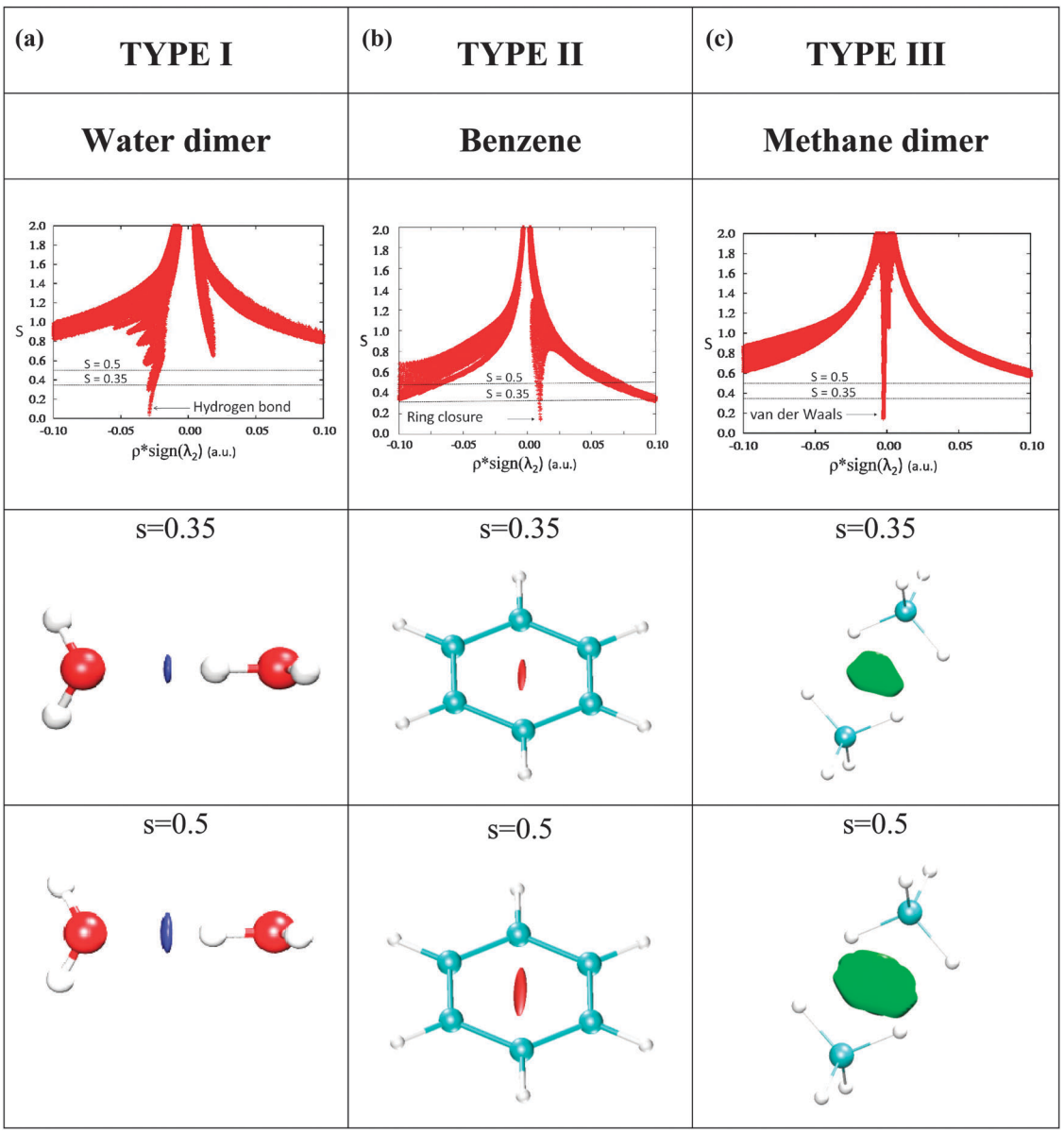

Fig. 1 Type I isosurface in the water dimer (a), type II isosurface in a benzene ring (b) and type III isosurface in the methane dimer (c).

idea is that spatial overlaps between atomic electron densities always generate local repulsive interactions, which in the case of stable systems are counterbalanced by attractive interactions, local or not. A classification of limiting cases is proposed as follows (note that density range values are just given for orientation):

(a) Strong stabilizing interactions (*e.g.* H-bond type)

When the local repulsion is counterbalanced by local inter- or intra-molecular attractive interactions, the net effect is stabilizing and a non-covalent bond takes place between the moieties concerned. This situation, which is referred to as type I NCI interactions, corresponds to the archetypal case of the H-bond, illustrated by the water dimer in its equilibrium geometry in Fig. 1a. In most of the cases previously investigated, this kind of interaction occurs between two atoms (*i.e.* the donor and the acceptor), being thus bicentric, directional and highly localized. In practice, such interactions typically correspond to values of $\rho > 0.01$ a.u. and $\lambda_2 < 0$. In this case, the stronger the interaction is, the larger the value of the electron density ρ at the trough. It should be noted that this kind of interaction is also characteristic of metallorganic interactions, which appear at an intermediate density in between covalent and non covalent.

(b) Strong destabilizing interactions (*e.g.* steric crowding)

When local repulsion is not counterbalanced by significant attractive local interactions, the adopted stable geometry does not only arise from interactions between atom pairs, but also from constraints external to them. This is the case when the repulsion is due to a sum of contributions from nearby atoms and is multicentric in essence. It is associated with a positive value of λ_2. This situation corresponds, for example, to steric crowding or ring closure,[65] as illustrated by the density overlap in the central part of a benzene ring as shown in Fig. 1b. It is referred to as type II NCI interactions. In practice, type II interactions are associated to values of $\rho > 0.01$ a.u. and $\lambda_2 > 0$. In the case of benzene, it can be viewed as a strain imposed by the ring structure, due to the covalent bonds responsible for ring cohesion. In the case of flexible molecules, such steric crowding can arise from structural constraints.

(c) Delocalized weak interactions (*e.g.* van der Waals)

Between these two limiting cases, a third type (referred to as type III) is considered. It gathers critical points found at very low density values and is assigned to much weaker interactions. In these regions, both density and gradient are small (typically $\rho < 0.01$ a.u., see Fig. 1c), and consequently λ_2 is also close to 0 ($\lambda_2 \sim 0$). In practice, this situation is most of the time encountered for weak attractive interactions like van der Waals forces. While each atom–atom contribution is weak, many atom pairs interact, which leads to a spatially extended zone describing the delocalized interaction. This interaction may thus significantly contribute to the total electronic energy, which is typically the case of van der Waals interactions as described in the methane dimer (Fig. 1c)

When λ_2 is too close to 0 (typically $|\lambda_2| < 0.0001$ a.u.), its sign is spatially unstable and its use becomes pointless: one should not rely on it to determine the local stabilizing or destabilizing nature of the interaction.

The 3D spatial visualisation of the non-covalent interactions as defined above is achieved from the 2D-plots, taken as input to construct 3D plots, *i.e.* isosurfaces of the reduced gradient of density. In a nutshell, a cut-off value of s close to zero, typically <0.5, is chosen in order to recover all the non-covalent interactions in the system, *i.e.* all the troughs of the 2D plots. The corresponding reduced density gradient isosurfaces give rise to closed domains in the molecular space which highlight the spatial localization of the interactions within the system. Since 3D isosurfaces are, by definition, regions of low reduced gradient, the density is nearly constant within these surfaces.

The s isovalue (or cut-off) chosen for plotting the 3-D isosurface determines which features will appear in the NCI plot as well as their spatial extension. On the one hand, all NCI troughs do not strictly achieve $s = 0$, so that too low a value might miss some of the interactions of interest. On the other hand, too high a value would disclose atomic tails of the density. The cut-off is therefore chosen from the 2D plot ($s = 0.35$ along this contribution) so that all troughs, but only troughs, are captured to render a meaningful picture which recovers both stabilizing and destabilizing interactions (see the more detailed discussion in the Technical appendix).

At this stage, however, the types of interaction corresponding to the several isosurfaces are not apparent. In order to discriminate between them, the density oriented by the sign of λ_2 is further used (as in the 2D plot). A RGB colouring scheme is chosen to rank interactions, where type II destabilizing interactions are coloured in red, type I stabilizing interactions in blue, and type III delocalized weak interactions in green. A marked intensity of the red and blue isosurfaces (*i.e.* a deeper colour) is associated to a higher local density and therefore to a stronger interaction.

With this procedure, type I interactions appear as compact and small, flat, pill-shaped blue isosurfaces, concentrated on the NCI critical point, with a colour going from blue-green to dark blue as the critical density increases (*cf.* the H-bond of Fig. 1a). The pill shape of these isosurfaces is due to the presence of two nearly degenerate negative eigenvalues in such bicentric interactions. Type II repulsions typically appear as red cigar-shaped surfaces, elongated along directions of decreasing density (*cf.* the central region of the benzene ring in Fig. 1b). Type III interactions correspond to greenish sheet-like extended forms indicating weak interactions (*cf.* van der Waals contacts in Fig. 1c).

The case of flexible complex molecules, exhibiting numerous intra- and inter-molecular interactions acting simultaneously, still requires a critical examination. It should indeed be mentioned that, in some rare cases, specific interactions appearing in NCI as type I interactions, and therefore labelled as ''stabilizing'', can be actually more complex than the basic NCI proposed classification. Such a situation can, for instance, be encountered in the case of steric clash, between a pair of atoms or in out-of-equilibrium dimers, even at medium range distances (see Technical appendix). In this case, NCI finds a critical point and, because of the bicentric nature of the interaction, the corresponding

NCI isosurface appears in blue, instead of red, despite the destabilizing nature of the interaction (which appears at greater values of $s(\rho)$, not analysed in the NCI regime). This usually happens because of non-equilibrium geometry of the system considered. However, in a large molecule, even in its equilibrium geometry, such situations can be encountered where the local structure does not correspond to a *local* equilibrium (because of a local steric clash for instance) but is stabilized by the rest of the system. This can also be the case in very constrained systems, with multiple competing intramolecular interactions. One motivation of this paper is then to perform a critical analysis of the performances of NCI when applied to these complex systems.

3. Application of the NCI approach to a flexible molecule: proof of principle

The NCI analysis has been carried out on a folded conformation (referred to as γ_L(g+)) of a flexible model system, *N*-acetyl-phenylalanyl-amide (NAPA). The NAPA molecule is known from gas-phase spectroscopy to exhibit a whole range of weak non-covalent interactions.[66,67] These interactions, as revealed from IR spectroscopy of the NH probes, range from a strong H-bond within the peptide backbone to a much weaker NH$\cdots\pi$ interaction between the peptide backbone and the benzene ring.

The 2D NCI-plot and the corresponding 3D NCI-plots are shown in Fig. 2 and can be analysed as follows:

– First of all, the strongest interaction, the intra-backbone H-bond, appears in the 3D NCI plot of Fig. 2 (top) as a well-defined pill-like type I flat isosurface of dark blue colour due to the high critical density value (ρ = 0.021 a.u.) as measured in the 2D plot. This high value of ρ at this NCI critical point reflects the strength of the interaction, in line with the significant red-shift of the NH stretch mode experimentally measured (120 cm^{-1}).[68]

– The other strong interaction, as testified by a high ρ critical value, turns out to be the signature of the benzene ring closure, which takes the form of a dark red cigar-shaped type II isosurface (ρ = 0.022 a.u.). It is not relevant in the present case for the analysis of intramolecular forces, since it pertains essentially to the stability of the benzene ring.

From the 2D analysis, the other interactions taking place in the molecule are expected to be weaker due to their lower critical electron densities.[21] Using this 2D plot to rank them, we can isolate, in the order of decreasing critical density:

(i) A series of three flat almond-shaped bicolour blue/red isosurfaces, with relatively dark colours indicating significant interactions, with critical ρ values in the 0.010–0.015 a.u. range. The blue parts of these isosurfaces are all associated with the presence of an intramolecular stabilising interaction, namely $^{\alpha}$CH$\cdots$OC, $^{\beta}$CH$\cdots$OC or NH$\cdots\pi$ interactions. These interactions are directional in nature and possess locally a significant bicentric character, hence the blue colour. One of them (NH$\cdots\pi$) is clearly observable in IR spectroscopy leading to a significant 30–50 cm^{-1} red-shift.[21–23,37,38,69,70] The same isosurfaces, however, also exhibit a red part, providing evidence

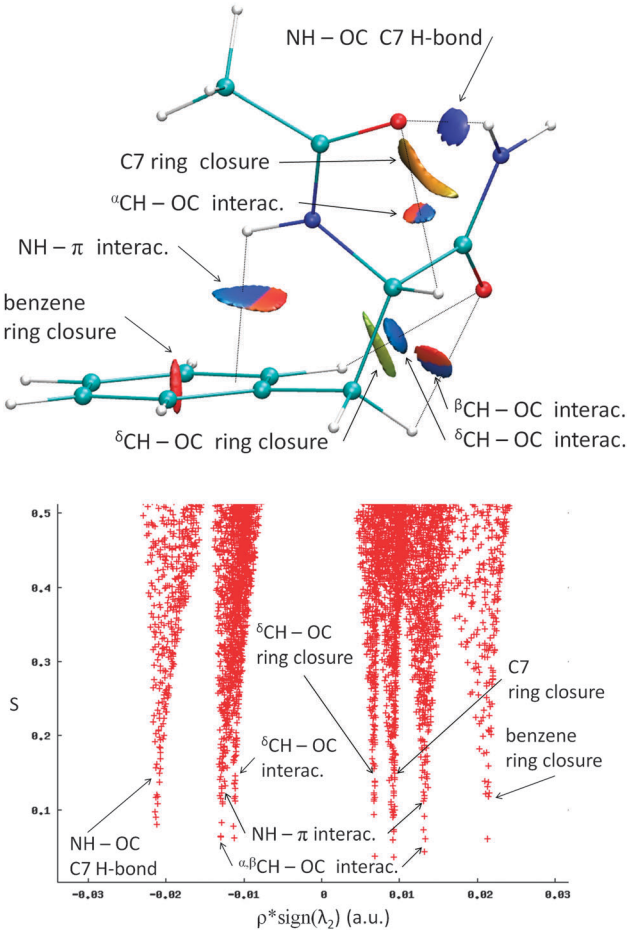

Fig. 2 3D (top) and 2D (bottom) NCI plots obtained for the γ_L(g+) conformer of the NAPA molecule.

for the multicentric character of the interaction, *i.e.* the steric strain induced by the formation of an intramolecular ring. These rings are 5-membered in the case of the first two interactions ($^{\alpha}$CH$\cdots$OC, $^{\beta}$CH$\cdots$OC). For the NH$\cdots\pi$ interaction, the ring is more loosely defined as the H atom interacting with the π system is actually close to both the $^{\gamma}$C and $^{\delta}$C atoms of the phenyl ring. This is reflected by the extension of the isosurface for this specific interaction. Such a bicoloured isosurface is thus assigned to the closure of an intramolecular ring, which results from stabilizing features (H-bonds, NH–π bonds) revealed by the blue colour, counterbalanced by destabilising interactions due to steric crowding within the ring, revealed by the red colour (Fig. 3). In the 2D NCI plots this dual character is reflected by the simultaneous existence of two symmetric or nearly symmetric twin troughs of opposite values of ρ sign(λ_2) as depicted in Fig. 2 (bottom). Such a mixed type of interaction will be labelled type I/II in the following, in reference to the coexistence of type I and II interactions in this feature.

(ii) In addition to the bicoloured almond-shaped isosurfaces, a pill-like light blue isosurface is also found at a comparable critical density (ρ = 0.011 a.u.). It corresponds to a $^{\delta}$CH$\cdots$OC interaction forming a 7-membered ring linking an amide carbonyl group and the phenyl ring. Although having a typical

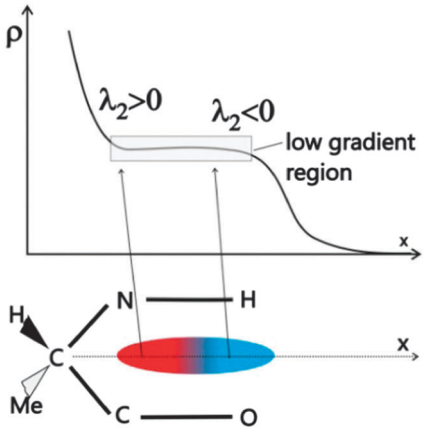

Fig. 3 Scheme of a type I/II 3D isosurface in a C5 ring formed in the groove between a carbonyl and a NH group within the same peptides residue in an extended β_L form. Along the groove the density does not vary significantly, hence the small gradient, the small reduced gradient and therefore the appearance of the 3D isosurface. Within this isosurface, however, the curvature varies significantly, leading to a blue external part illustrating the directional NH···O interaction, whereas the red part is indicative of the strain in the 5-membered ring resulting from a multicentric density in the inner region close to the backbone. In the top panel the variation of the density and the sign of λ_2 along the valley between the CO and NH groups is depicted.

type I shape, it is clearly much weaker than the regular H-bond as indicated by the light-blue colour. It also illustrates a case where NCI notices the presence of a weak interaction for which it is difficult to predict the stabilising or destabilizing character as discussed earlier in Section 2. It could, for instance, correspond to a slightly repulsive interaction, like in the medium distance ammonia dimer, described in the Technical appendix. The present molecular context, however, helps to understand the type of interaction: the aromatic $^{\delta}$CH is pointing to an electronegative atom suggesting a weakly attractive H-bond-like interaction.

(iii) Finally, two elongated, ''cigar-like'' features are also encountered for very small ρ critical values ($\rho < 0.01$ a.u.). Their shape is comparable, although less symmetrical, to the signature of the benzene ring closure: each isosurface is nearly centred relative to an intramolecular ring and roughly oriented perpendicularly to the average plane of this ring. They correspond to the closure of the intra-backbone seven-membered ring (C7 H-bond) and of the backbone-phenyl seven-membered ($^{\delta}$CH···OC) ring. However, their critical ρ values, much smaller than in the benzene ring, reflects a much smaller strain. These critical ρ values also differ from each other: it is larger in the most crowded intra-backbone C7 ring (with a yellowish banana-shaped surface) compared to the backbone-phenyl 7-membered ring (green cigar). The colour of the former surface qualifies it as a slightly destabilising NCI type II interaction whereas the green latter one would classify it among the weak, less significant type III interactions.

The example of NAPA shows that the NCI procedure enables us to rank the several interactions according to their type and strength, with special attention to the intramolecular ring resulting from the interactions considered.

– In strong bidirectional (blue) interactions, typically H-bonds linking remote groups along the backbone, the ring formed is usually large ($\geq$7 atoms). As a consequence the weak strain imposed to the backbone is described as a barely significant green cigar-like isosurface, characteristic of the topological signature of the ring. This case gives rise to two distinct isosurfaces of type I on one hand and of type II or III on the other hand.

– Weaker bidirectional (light-blue) interactions (type I/II), in contrast, are hampered by significant backbone strains because the ring formed is usually short (typically 5-membered). This gives rise to bicolour isosurfaces indicating neighbouring bidirectional stabilising and multicentric destabilising interactions.

These two limiting cases are topologically equivalent; the difference essentially rests on the spatial separation of the stabilizing and destabilizing components. All kinds of intermediate cases should be expected, depending on the strength of the interaction responsible for the ring closure as well as on the ring length.

This present detailed analysis of a typical folded system of biological relevance demonstrates the ability of the NCI procedure to visualize and describe the intramolecular interactions at play in such a flexible molecule. It will be extended in what follows to the analysis of comparable flexible molecules of spectroscopic interest and of their complexes.

4. Application of the NCI approach to observed intramolecular interactions

After this proof of principle, we illustrate how to use the 3D and 2D NCI plots on systems of increasing size exhibiting intramolecular hydrogen bonds. Indeed, such systems show special interest as their structures result from a subtle balance between several competing interactions. As they have been fully characterized experimentally, they provide a good test for NCI representations. In this section, we will first focus on an aminoalcohol, a small system with a limited number of non-covalent interactions including a single OH···N or NH···O hydrogen bond. We will then move on to small peptides which are more complicated systems exhibiting complex networks of competing interactions ranging from the weakest NH···π interaction to stronger H-bonds. All these systems have had their conformational landscape fully characterised in the gas phase. Each stable conformation can be isolated in a supersonic expansion and characterized by combining IR and UV spectroscopy in so-called IR/UV double resonance experiments. Each form is identified from its UV features and its structure is determined from the comparison between the conformer-selective IR spectra obtained and that simulated by quantum chemistry calculations.

4.1. (*S*) 1,2,3,4-Tetrahydro-3-isoquinoline methanol (THIQM) as an example of 1,3 aminoalcohol

Intramolecular OH···N hydrogen bonds such as observed in 1,2 or 1,3 aminoalcohols are usually characterised by smaller spectroscopic shifts of the ν(OH) stretch mode than those

observed in intermolecular OH···N interactions.[71] These smaller shifts reflect weaker H-bonds frustrated by the steric constraints brought by the backbone geometry.

Aminoalcohols exist in two conformers showing OH···N or NH···O interactions. In most cases, the NH···O hydrogen bonded conformer is calculated at a higher energy. This is easily understandable as OH is a better hydrogen bond donor and a poorer acceptor than NH_2. However, the NH···O conformer can be stabilised in peculiar situations, for example by complexation with an appropriate hydrogen bond donor[51,52,72] or in molecules whose stereochemistry makes the NH···O interaction sterically possible. This has been achieved in 1,2,3,4-tetrahydro-3-isoquinoline methanol (THIQM). THIQM (Fig. 4) is built from a benzene ring fused with a six-membered aliphatic ring containing a nitrogen atom in position 3. The six-membered aliphatic ring also contains a methanol substituent in position 2. While the most stable conformation of the latter is in the equatorial position, there are two non-equivalent minima with the amino group hydrogen–lone pair either in axial–equatorial or in equatorial–axial positions, respectively.[73]

The two resulting conformers strongly differ from each other (Fig. 4). The most stable $THIQM_I$ conformer with the nitrogen lone pair in equatorial position shows an OH···N interaction while the less stable $THIQM_{II}$ conformer with the lone pair in axial position shows the opposite NH···O interaction. Both of them are observed in jet-cooled conditions and spectroscopically characterised by the value of their ν(OH) stretch frequency (free ν(OH) at 3686 cm^{-1} in $THIQM_{II}$ *vs.* bound ν(OH) stretch mode in $THIQM_I$ at 3566 cm^{-1}).

Both conformers exhibit similar 3D NCI isosurfaces (Fig. 4a), with a type II isosurface at the centre of the benzene or six-membered aliphatic ring, illustrating the ring strain. The H bond is characterised by the typical type I/II bicolour surface denoting two competing effects, between the attractive interaction and destabilizing crowding effect.

The differences in terms of intramolecular hydrogen bonds between $THIQM_I$ and $THIQM_{II}$ are clearly evidenced in the 3D isosurfaces shown in Fig. 4b, as differences in the type I/II surface. $THIQM_I$ shows a strongly contrasted from blue-to-red isosurface, in line with an OH···N interaction of appreciable strength (d(H···N) = 236 pm). Conversely, the isosurface describing the NH···O interaction in $THIQM_{II}$ shows a less clear contrast, reflecting the weaker NH···O hydrogen bond (d(H···O) = 245 pm). The aspect of these two isosurfaces provides direct visual comparison between the two conformers and allows immediate assessment of the strength of the intramolecular bond (blue-green part of the surface) and the tightness of the covalent ring binding the two heavy atoms involved (red-yellow part of the surface).

The 2D NCI diagrams of Fig. 4a confirm this view. The two conformers have in common two troughs in the repulsive interaction region, with ρ values of about 0.02 a.u., corresponding to the strain in the two covalent rings. In contrast, they show substantial differences in regions of lower density although both exhibit twin symmetric troughs in the attractive (negative λ_2) and repulsive parts (positive λ_2) of the 2D plot (Fig. 4b) as expected for a type I–II interaction. The critical density values are quite different: 0.0154 a.u. for $THIQM_I$ *vs.* 0.0112 a.u. for $THIQM_{II}$, in agreement with the experimental findings of a stronger hydrogen bond in $THIQM_I$ relative to $THIQM_{II}$. This confirms the respective hydrogen bond acceptor and donor abilities of NH and OH. The stronger interaction results in turn in a tighter ring with a more positive value of ρ in the intramolecular hydrogen bond region in $THIQM_I$ relative to that in $THIQM_{II}$.

4.2. Applications to short peptides for a local modeling of protein chains: intrabackbone H-bonding in peptides (secondary structures)

Intrabackbone H-bonds are the keys of the secondary structures of proteins. Using a gas-phase approach, they have been successfully documented in isolated model peptide molecules by IR spectroscopy.[20,21,24,30,38,39,66,67,69,74–81] More precisely, the exquisite sensitivity of the NH stretch frequency to its local environment, made possible by the weak coupling between the several NH stretches of the molecules, provides invaluable structural information and allows a determination of the structure of all the conformers present in the expansion. A whole range of interactions between an NH moiety and more or less remote amide CO bonds along the chain (usually an H-bond) have been identified and labelled as C*n* according to the number of atoms (*n*) involved in the ring closed by the interaction (Fig. 5). One can distinguish local interactions, spanning essentially around a unique residue and its bracketing amides, namely,

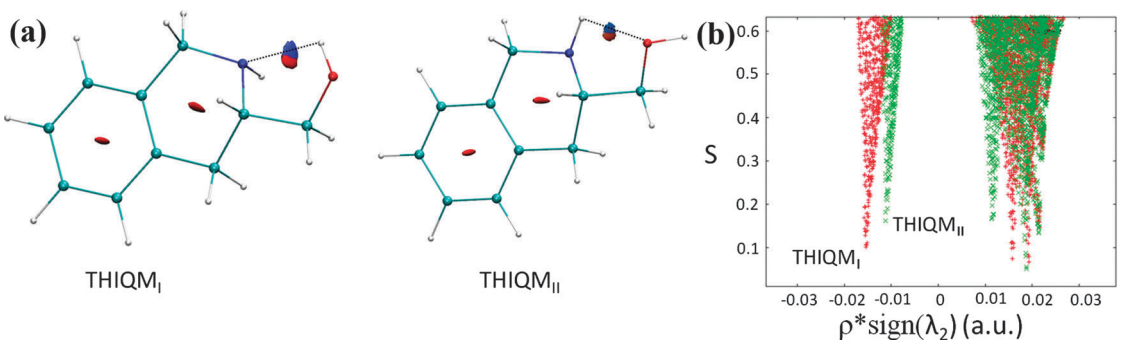

Fig. 4 (a) 2D and (b) 3D NCI plot obtained for the THIQM stable conformers.

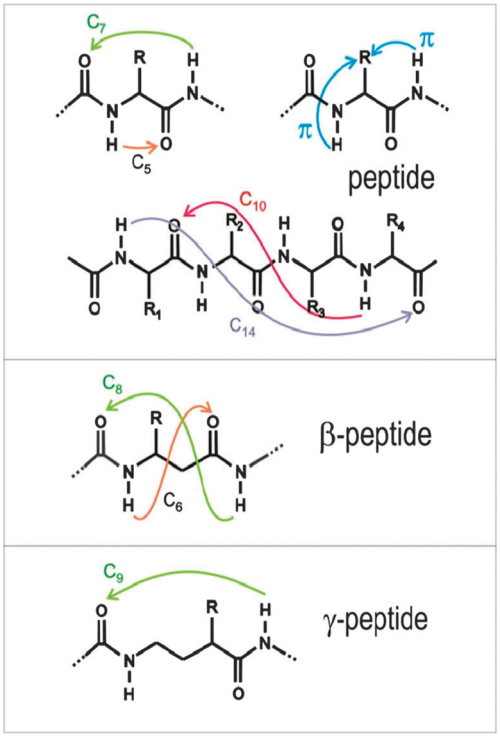

Fig. 5 Folding schemes of α-, β- and γ-peptides, with their characteristic H-bonds and interactions.

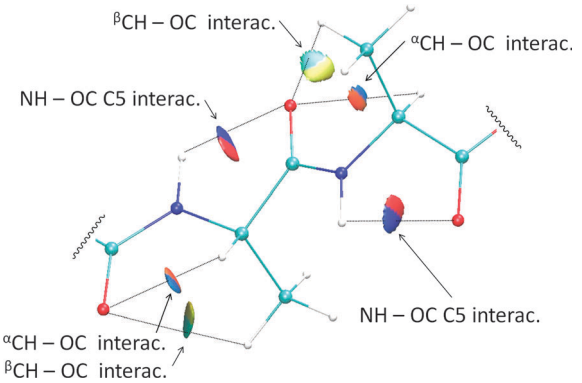

Fig. 6 Example of two C_5 interactions in the β-strand-like extended conformation of Ac-$(Ala)_2$-OBzl, with accompanying $^{\alpha}$CH···OC and $^{\beta}$CH···OC weak H-bonds.[20]

C5 and C7 interactions in (α-)peptides, C6 and C8 in β-peptides, and C9 in γ-peptides (Fig. 5). Beyond this, involving more than one residue, one finds C10, C13 and C14 interactions in α-peptides, C11 in β-peptides, *etc.*... From a general point of view, these interactions strongly differ in their geometrical and spectroscopic features. C5, C6 interactions are weak because they are constrained by the peptide backbone geometry, and they lead to modest red-shifts of the NH stretching vibration, whereas interactions involving several residues exhibit the typical features of classical H-bonds: they are more linear and can be easily characterized from their IR spectroscopic features: red-shift, band broadening and enhanced oscillator strength, typical of moderate to strong H bonds.

The aim of the present section is twofold: it will first illustrate the interest of the NCI procedure as a method to efficiently visualise the interactions observed by spectroscopy in these exemplary secondary structures of proteins as well as to help ranking them according to their strength. Second, it will give access to interactions which cannot be directly evidenced experimentally, bringing new insights into the physics underlying the structure of these systems.

(a) The β-strand: an example of constrained C5 NH···OC bond. Extended conformations of peptides (typically β-strands) are stabilized by NH···OC C5 interactions, linking the NH and the CO of the same residue in a quasi-planar arrangement (Fig. 6).[20,24,30,67,78] The closure of this C5 ring gives rise to a type I/II NCI isosurface (found at $\rho \approx 0.016$ a.u.). Its external part (of blue-green colour) is centred on the line joining the oxygen atom of the carbonyl group to the H atom of the NH group; it emphasises the significant interaction between these H and O atoms. The other (inner) part of the pill extends towards the backbone due to the overlapping contributions from the series of atoms forming the C5 ring, in a situation identical to that described in Fig. 3. The resulting steric crowding is responsible for the reddish colour of the pill in the groove between the CO and NH groups.

Interestingly, interactions which are not experimentally evidenced (see below) are revealed by NCI: these extended β-strand structures are additionally stabilized by minor H-bonds between neighbouring $^{\alpha}$CH and $^{\beta}$CH groups and the CO moiety of the previous residue along the chain (Fig. 6). Similar bicoloured type I/II features occur, characteristic of the closure of the corresponding C5 or C6 membered rings, but in this case, however, the green and orange colours indicate a much weaker interaction (found at 0.0115 a.u. in the 2D plot – not shown).

From a spectroscopic point of view, the NH···OC C5 interactions are known to lead to modest red-shifts (typically 40 cm^{-1}) of the NH stretch frequency, in line with the non-linear NH···O pattern.[20,30,67,78] This shift encompasses the whole complexity of the interaction at play, whereas NCI allows a disentangling of its multiple components; it reveals the multicentric character of this peculiar H-bond. Concerning the weaker CH···OC interactions, their effect on the CH stretch spectroscopy is difficult to quantify because of their weakness and of the strong coupling between the CH oscillators of the molecule, whereas the interaction appears clearly on the 3D NCI plots.

(b) γ-turns, as examples of intramolecular C7 rings. Among γ-turns, *i.e.* intra-backbone rings stabilized by C7 H-bonds, inverse γ-turns (γ_L) are archetypal secondary structures, ubiquitous in natural peptide chains. They correspond in particular to the γ_L Ramachandran backbone orientation in natural L-conformation residues, which causes the residue side chain to lie in an equatorial position relative to the C7 ring. Many such turns have been reported in the literature for isolated peptides, with sizes ranging from capped amino acids up to pentapeptides.[20,21,24,30,37,39,67,76,79] The γ_L conformation of the NAPA molecule, chosen as the proof of principle, is an example of such structures. For the sake of illustration, a simple example is found in the γ_L conformation of the Ac-Ala-NH-Me-capped alanine (Fig. 7).

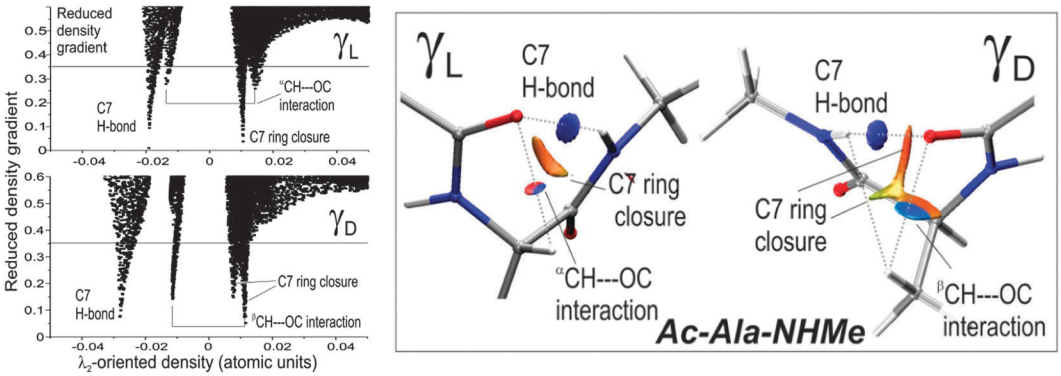

Fig. 7 Comparison between the γ_L- and γ_D-turns of Ac-Ala-NHMe. 2D NCI plots (left); 3D NCI-plots (right): reduced density gradient isosurfaces (at s = 0.35), as obtained from the analysis of B97-D/TZVP optimized structures.

The 3D NCI surfaces for this conformation provides three distinct features at very different NCI critical densities:

– A dark blue type I isosurface of high density, corresponding to the significantly strong C7 H-bond ($\rho \sim 0.19$ a.u.).

– A type I/II isosurface, featuring the existence of a secondary ring C5, based on the interaction between the oxygen atom of the acetyl carbonyl group and the H atom of the $H^{\alpha}C$ bond. It is characterized by a blue part of the critical density ($\rho \sim 0.14$ a.u., hence the light blue colour) accompanied by the red extension towards the backbone characteristic of a ring closure. This weaker $^{\alpha}CH\cdots OC$ interaction (interatomic distance 253 pm) is made possible by the existence of the H atom in the axial position with respect to the main C7 ring; the side chain being in an equatorial position in such γ_L-turns.

– Finally an elongated reddish (type II) isosurface of weak density ($\rho \sim 0.011$ a.u., hence the pale red colour) associated to the C7 ring closure, similar to that mentioned in the NAPA analysis (Fig. 2). It should be assigned to weaker interactions due to simple contacts and/or to diffuse multicentric interactions.

Besides the γ_L turns previously described, peptides can adopt conformations with opposite backbone chirality, namely direct (γ_D) turns. The main difference between the two structures lies in the conformation of the side chain relative to the mean plane defined by the C7 ring, *i.e.*, equatorial for inverse and axial for γ_L-turns.

An example is given in Fig. 7, the γ_D conformation of Ac-Ala-NHMe. Even if they share the same type of C7 H-bond with γ_L-turns, γ_D-turns are usually significantly less stable (in Ac-Ala-NHMe, by 2.1 kcal mol^{-1}, including ZPE-correction), hence less common in proteins. However, their H-bond seems to be stronger, as suggested by both the calculated H-bond distances and experimental NH frequencies.[21] This apparent contradiction reveals that the H bond is not the decisive contribution to the overall stability and that additional interactions, not evidenced spectroscopically, also play a significant role. The NCI-plot analysis provides a convenient way to distinguish the differences in intramolecular interactions between γ_L and γ_D turns.

The 2D NCI-plots (Fig. 7 left) first show that the critical densities for the C7 H-bond are significantly different (ρ = 0.028 a.u. in γ_D *vs.* 0.019 a.u. in γ_L). They scale with the spectroscopic red-shift measured on the two types of turns: the H-bond of the γ_D-turn being slightly shorter (calculated NH$\cdots$O=C distance of 192 pm) and stronger (experimental NH stretch frequency of 3340 cm^{-1}) than that of the γ_L-turn (211 pm and 3370 cm^{-1} respectively).[21] The secondary interactions however are also different. Due to the axial position of the side chain, the type I/II $^{\alpha}CH\cdots OC$ interaction (5-membered ring) present in γ_L is not possible. It is replaced by a C6 ring interaction corresponding to a type I/II $^{\beta}CH\cdots OC$ (CH$\cdots$O=C distance of 253 pm) in γ_D. The latter is probably weaker as suggested by critical densities ($\sim$0.0115 a.u. in γ_D *vs.* $\sim$0.014 a.u. in γ_L). Moreover, an additional difference arises from the different shapes and critical densities of the type II isosurfaces located in the central area of the turns. Although still elongated, it appears to be more extended in the γ_D-turn with a slightly larger density in its central part ($\sim$0.0115 a.u. in γ_D *vs.* $\sim$0.0105 a.u. in γ_L), prolonged by a type III (green; $\rho \sim$ 0.08 a.u.) spike pointing to the empty space between the H-bond and the side chain, and with one edge partially merging with the red part of the $^{\beta}CH\cdots OC$ type I/II isosurface.

All these features offer a way to rationalize the relative stabilities observed in favour of the γ_L-turns: in spite of a (relatively) weaker H-bond, this structure probably benefits from significant stronger ancillary interactions, in particular the $^{\alpha}CH\cdots OC$ interaction.

(c) β-turns, with C_{10} H-bonds. The β-turn is an important secondary structure of nature, allowing peptide chains of protein to fold upon themselves. It is illustrated here on the model Ac-$(Gly)_2$-NH_2 system (Fig. 8). It is stabilised by a C10 H-bond, characterised by a type I dark blue isosurface with a strong critical density (ρ = 0.018 a.u), in agreement with the significant red shift (90–110 cm^{-1}) of the NH stretch frequency measured.[38,69,76,77,82] NCI, however, reveals additional interactions which contribute to the turn stability. The NH engaged in the C10 H-bond also interacts significantly with the N atom of the central amide (Fig. 8), giving rise to a constrained 5-membered NH$\cdots$N ring, with a characteristic type I/II isosurface (ρ = 0.014 a.u.). A complementary 7-membered ring, closed by both the H-bond and the NH$\cdots$N interaction is observed. The topological signatures of the C10 ring closure are located in the middle of these 5- and 7 membered rings,

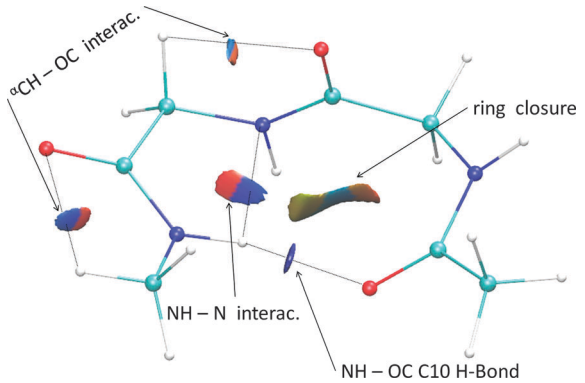

Fig. 8 3D NCI plot of a type II β-turn conformation of the Ac-$(Gly)_2$-NHMe model peptide, extracted and adapted from the most stable form of Ac-$(Ala)_4$-O-Bzl.[79]

i.e., for the former, the red part of the type I/II isosurface and, for the latter, of a distorted type III pale multicolour isosurface, signing very weak interactions associated to a very low density, to which contributes a weak CO···OC steric clash between the central and the C-terminal carbonyls.

(d) Other H-bonds in a crowded environment: signature of a ring closure. Different types of turns in α-, β- and γ-peptides (Fig. 9) can also benefit from a NCI analysis. C6, C8, C9 rings closed by NH···OC H-bonds involve similar type I NH···OC, type I/II CH···OC and type III interactions. Examples of these structures have been recently described from double resonance IR/UV experiments and assigned by comparison with quantum chemistry calculations. These turns are all based on a strong H-bond, giving rise to blue type I isosurfaces, with ρ values ranging from 0.0165 a.u. for C6 to 0.024 a.u. for C9. These conformations are additionally stabilized by type I/II interactions, either a $^{\alpha}$CH···OC interaction for the C8 β-[74] and C9 γ-species[80] or a $^{\beta}$CH···OC interaction in the C7 axial (γ_D turn of an α-peptide) form.[21] The β-C6 form stands apart in the series due to the absence of such CH···OC type I/II close contacts, because of the compact methylene spacers, and its relatively short length (six membered), making it not flexible enough to allow close contacts between the remote parts of the ring. This topological singularity forbids any additional type I/II stabilizing interaction.

In addition to type I and I/II interactions, type III features are always found in these turns, elongated and orientated roughly perpendicularly to the ring plane, with a size increasing with the side chain volume. The central region of the turn involves multiple interactions, which contribute to a multicentric building up of the electron density, leading to these greenish isosurfaces. Their spatial extension should be considered as a qualitative assessment of this effect.

(e) NH···π interactions. NH···π interactions are ubiquitous in peptides and proteins. In gas phase neutral structures, they often appear as auxiliary stabilizing interactions, made possible by the proximity of a free amide NH bond and the π system of an aromatic side chain. They are even capable of orienting the backbone structure and mediating the competition between secondary structures in capped di- or tri-peptides.[40,68] In this context, NCI provides a way to characterize and distinguish them. In order to illustrate this, we will focus on two conformations, observed in the gas phase, in which a folded backbone enables such interactions to form:

(i) The γ_L(g+) form of NAPA, already discussed in Section 4.2.2., provides a nice example of a strong interaction of an amide NH with the Phe side chain to the same residue, made possible by the locally folded backbone (Fig. 10, left). The corresponding crowded region is detected by NCI through a typical type I/II isosurface, characterized by a critical value of 0.013 a.u.

(ii) The most stable form of the Ac-Ala-Ala-O-Bzl molecule[82] (A2b in short) exhibits a NH···π interaction involving the two

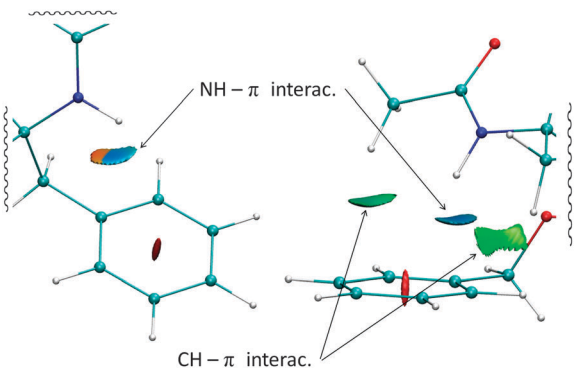

Fig. 10 Examples of NH···π interactions in isolated peptides; (left) NAPA γ_L(g+) conformation;[67] (right) folded conformer of the Ac-$(Ala)_2$-O-Bzl molecule.[82]

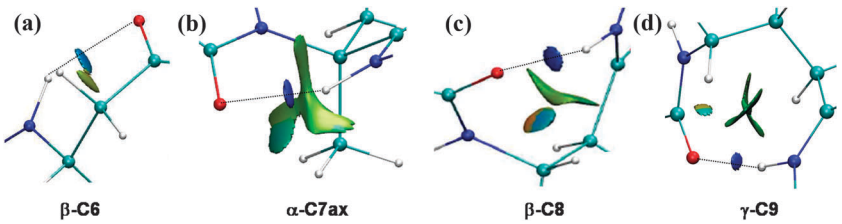

Fig. 9 (a) C6 ring in the two most stable C6a(1) form of the Ac-β^3-hPhe-NHMe β-peptide molecule assigned by Zwier and coworkers[74] to the most abundant conformer (A) of this species in the gas phase; (b) C7 ring in the presence of an axial side chain in the γ_L conformation of the Ac-Aib-NH_2 α-peptide, causing a C6 $^{\beta}$CH···OC interaction to take place;[21] (c) C8 ring in the conformation C8b(3) of Ac-β^3-hPhe-NHMe, found to give the best agreement with the experimental data of conformer B reported in ref. 74; (d) C_9 ring in conformer C9(a) of Ac-β^3-hPhe-NH-Me found to fit conformer A as experimentally observed.[81]

ends of the molecule: the NH of the first Ala residue and the aromatic benzyl ring. In this case, however, because of the much longer chain the constraints are reduced and the NH bond points more directly towards the phenyl ring, leading to a type I/type III (delocalized but notably strong interaction) NCI flat, blue isosurface ($\rho \sim 0.0095$ a.u.), whose shape adopts the π cloud local curvature. Also similar is the interaction between the methyl moiety of the acetyl group and the phenyl ring, which gives rise to a blue-green isosurface ($\rho \sim 0.0055$ a.u.), to be related to the dispersive interaction between methyl and phenyl groups. Finally, in this overall folded molecule, these still significant NCI signatures are accompanied by multiple type III green isosurfaces of barely significant density values ($\rho \sim 0.003$ a.u.), to be assigned to the topological closure of the loose intramolecular rings.

The strength of the π H-bonds, illustrated by red-shifts of the NH stretch frequency in the 40–50 cm^{-1} range (NAPA 3438 cm^{-1};[67] A2b: 3429 cm^{-1},[82] with an unperturbed free NH at 3480 cm^{-1}), is in line with the significant critical values of the density obtained (see above). One will, however, notice that a larger shift is observed for the A2b molecule, in spite of its lesser critical density. This example illustrates the fact that the density at the critical point may not be the unique relevant parameter controlling the strength of such spatially extended and multicentric interactions.

5. Applications to chiral recognition: specific interactions in diastereomer complexes

Chiral recognition is thought to happen through the formation of weakly bound complexes involving specific interactions.[83] Spectroscopic characterization of these weakly bound neutral[46,84] or ionic[54,85] complexes isolated in the gas phase allows a better comprehension of the interactions responsible for chiral recognition without the perturbation brought by the solvent. Chiral recognition results from a subtle balance between a plethora of weak interactions which are difficult to unravel.[86] Especially challenging is the fact that recognition is usually better in less strongly bound complexes, as shown recently in supramolecular chemistry experiments.[87,88] This points to the fact that chiral recognition is usually not directly related to the strongest interactions ensuring the stability of the complex, but results from much weaker specific interactions, such as CH···π, CH···O, or differences in dispersion between the two enantiomers. Dramatic differences have been sometimes observed in binding patterns, with a change in the hydrogen bond nature[51,52,72] or pattern,[89,90] a swap from hydrogen bond to dispersion between two enantiomers,[53] or a change in the interaction site with a cation.[27] However, this situation is rare and most of the examples of chiral recognition reported so far rest on tenuous differences between the two diastereomer complexes,[41,42,44,45,49,91–95] which can be, however, spectroscopically observed. There is therefore a need for theoretical methods enabling the visualization of weak interactions and their dependence upon chirality.

We present here a typical case of chiral recognition in neutral complexes, whose interaction pattern has been documented by gas phase laser spectroscopy.[42,54,73,96,97]

The (1*S*,2*R*)-(−)-*cis*-1-amino-2-indanol (AI)–methyl lactate (ML) diastereomeric complexes have been extensively studied by IR-UV double resonance experiments.[54,73,96] The most important result of these studies is that each diastereomer complex exists in two distinct isomeric forms. On the one hand, the same insertion structure is formed in the complexes between (1*S*,2*R*)-(−)-*cis*-1-amino-indan-2-ol and the two enantiomers of methyl-lactate, with similar binding energies and spectroscopic signatures. On the other hand, a unique addition complex is formed for *R* methyl-lactate, called heterochiral hereafter, because the corresponding complex with *S* methyl-lactate (called homochiral) is much less stable. This selectivity rests on the formation of a weak CH···π interaction which is not possible for the other enantiomer. In what follows, we shall focus on the latter structures which are depicted in Fig. 11 (top).

Visual examination of Fig. 11 qualitatively explains why the heterochiral addition complex is more stable than the homochiral one, despite a similar main binding interaction (OH···O hydrogen bond). Indeed, changing the methyl-lactate chirality only consists in swapping the H atom on the asymmetric carbon and the methyl group. This change introduces repulsion, prevents the formation of a CH···π interaction, and decreases the binding energy by 2 kcal mol^{-1}, a value usually associated with CH···π interactions. However, no direct signature of this critical interaction was observed so far, because it has only a limited and hardly predictable influence on the ν(CH) stretch frequency.[2,98] Fig. 11 illustrates how NCI allows unravelling the different interactions postulated in the diastereomer complexes. The positive λ_2 region corresponds to the benzene and C5 aliphatic ring strains, which appear at similar ρ values for the two diastereomers and for bare amino-indanol (not shown). The negative λ_2 region contains again the intramolecular interaction, which is seen at $\rho = 0.0269$ a.u. in bare amino-indanol. They are observed in the complexes at slightly larger values: $\rho = 0.0334$ a.u. and 0.0265 a.u. for the homo and heterochiral complexes, respectively, which shows that the intramolecular interaction is reinforced by the formation of the intermolecular OH···O hydrogen bond in the homochiral complex, while it remains about the same in the heterochiral complex. The intermolecular OH···O interaction appears in the same region, in line with similar frequencies for the inter- and intra-molecular stretches. It is observed at 0.0353 and 0.0334 a.u. for the homo and heterochiral complexes, respectively. However, the values of the density in this range are very close to each other and the 2-D plot is not unambiguous. The 3-D isosurface allows disentangling these two interactions which cannot be distinguished spectroscopically or by the 2-D plot. Indeed, the intramolecular bond is characterised by the typical type I/II isosurface. In contrast, the intermolecular hydrogen bond is more favourable sterically and corresponds to a typical type I isosurface.

We shall now focus on the region closer to $\rho = 0$. The two diastereomers have in common two deep and broad troughs corresponding to the dispersive interactions between the

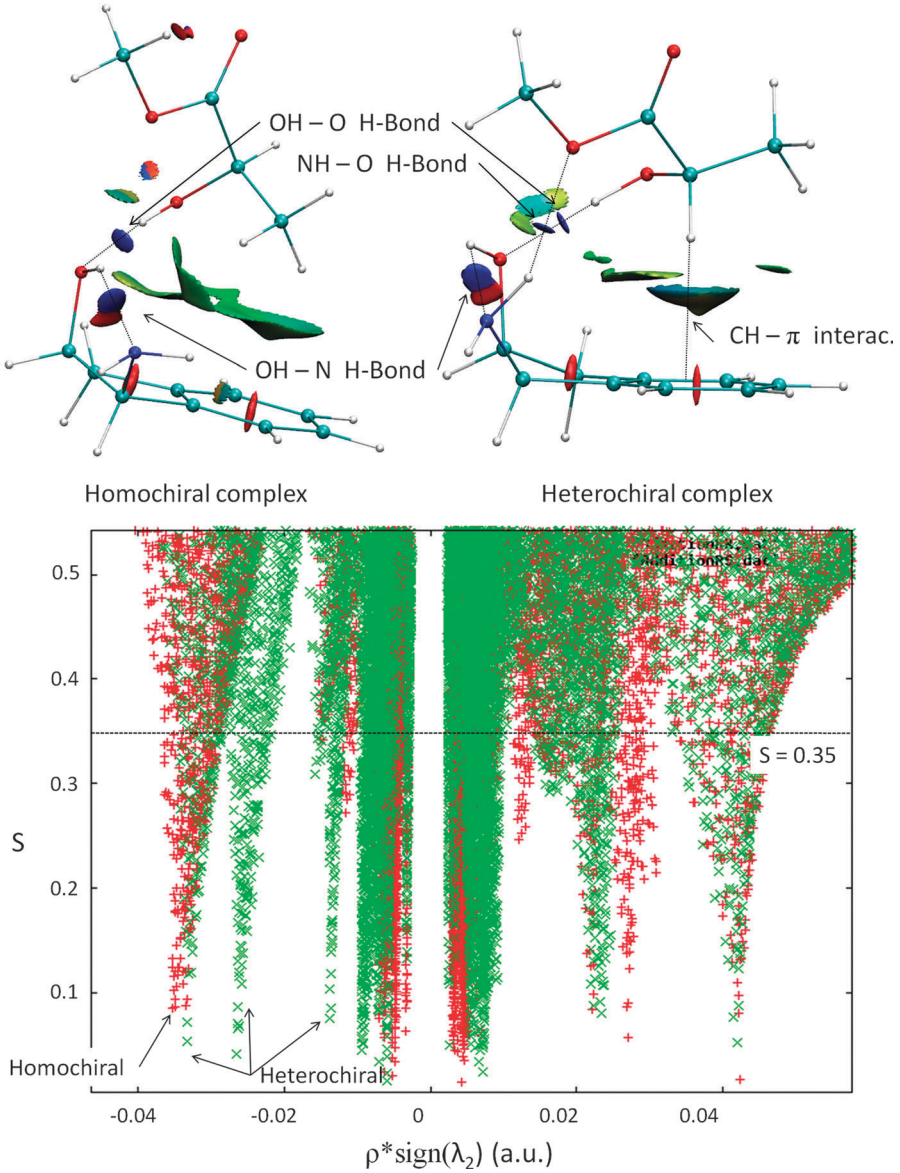

Fig. 11 3D-NCI plots (top) and 2D-NCI plots (bottom) of the heterochiral and homochiral (1*S*,2*R*)-(−)-*cis*-1-amino-2-indanol–methyl lactate complexes.

chromophore and the alkyl chain and the ester group of methyl-lactate, respectively. They are visualised as green flat type III isosurfaces; the large sheet corresponds to the interaction between the methyl-lactate alkyl group and the AI benzene ring while the small one visualises the interaction between the methyl-lactate ester and the AI benzene ring.

The most interesting region of the 2-D plots is at a slightly negative value of λ_2. Indeed this region is very different for the two complexes. Two deep and narrow troughs appear in this region for the heterochiral complex only. A first critical point is observed at 0.0094 a.u. and corresponds to the postulated CH$\cdots\pi$ interaction. It is visualised as a blue-green gradation in the dispersion domain characterising the alkyl-chromophore dispersive interaction. Note that such a gradation is not observed for the other diastereomer, which exhibits a green type III surface. The second trough lies at 0.0139 a.u. It has been assigned to a weak NH$\cdots$O interaction between the amino group of AI and the methoxy of methyl lactate. It is visualised as a pale blue type I disk between NH and OCH_3. Its smaller extension shows that this weak interaction is bicentric and localised, in contrast with the CH$\cdots\pi$ interaction formerly discussed. It is also worth noticing that this interaction was neither observed (because of the weak spectral signatures of the NH$\cdots$O bonds in amino groups) nor postulated in our experimental work,[54,73] which illustrates the complementarity of the NCI plot visualisation with the spectroscopic approach.

6. Conclusion

In this contribution, we have shown that the recently-developed NCI technique provides an in depth understanding of the

various types of interactions present in complex systems in combination with experimental results from gas phase spectroscopy. The presence of intra- and inter-molecular interactions in molecules chosen among molecular neutral systems exhibiting a large diversity of interactions, in particular inter- and intramolecular hydrogen bonds, and for which an unambiguous structural determination was achieved using state-of-the-art conformer-specific vibrational spectroscopy was documented using NCI. The revealed interactions range from weak intramolecular H-bonds in a simple amino-alcohol to complex bonding patterns observed in model peptides of increasing sizes and complexity. Finally the NCI technique successfully accounts for chiral recognition in model isolated systems. These examples demonstrate that the NCI approach allows spectroscopists to provide an elegant visualization of the interactions that potentially impact their spectroscopic vibrational probes, namely the OH and NH stretching motions. These qualitative results clearly highlight the capability of a quantum interpretative technique to help the experimentalists to unveil key interactions influencing the geometries and vibrational frequencies in systems difficult to interpret. Future work will focus on the quantitative use of such quantum interpretative techniques to facilitate the spectroscopic assignments.

Technical appendix

(1) Choice of cut-off

In this contribution, a cut-off of 0.35 was taken in order to capture the whole range of interactions for the present series of systems. Of course, the adequate cut-off would be system-dependent. In practice we kept the cutoff low enough to visualize the main interacting partners within the NCI regime: *i.e.* low density associated to low reduced density gradient.

With larger cutoffs (*i.e.* 0.4–0.6), additional isosurfaces corresponding to non-NCI interactions and associated to regions of higher density begin to appear. In that case, as we are beyond the range of applicability of the NCI method, other methods especially designed to highlight regions of strong electron pairing should be preferred, such as the topological analysis of the electron localization function.[99–102]

(2) Interpretation of NCI for non-equilibrium systems

Usually NCI should be used to reveal weak interactions. However the synergistic use of both density and reduced density gradient can be applied to stronger interactions like covalent bonding.[103] In particular cases, the global stability of a system is not solely governed by the weak non-covalent interactions, especially in the case of strong steric clashes or in the repulsive configuration of the ammonia dimer (Fig. 12a and b). In the latter system, where the two nitrogen atoms are facing each other, the long range interaction is dominated by van der Waals-type forces (type III green isosurface). At medium range the interaction becomes stronger and more attractive. At still shorter distances, the conformation eventually exhibits a dark blue isosurface, whereas the conformation is repulsive, with positive global interaction energy.

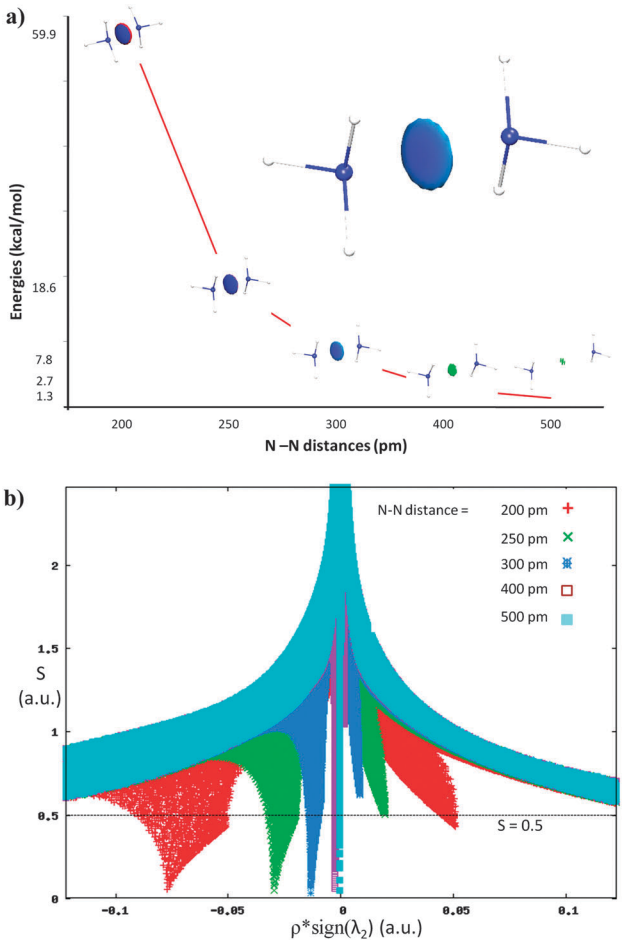

Fig. 12 (a) Interaction energy of the NH_3 dimer in a repulsive conformation, as a function of the N···N distance, together with the 3D NCI plots showing a type I isosurface; (b) corresponding 2D NCI plots for different N···N distances.

While the behaviour of the systems at intermolecular distances beyond 300 pm can be easily understood within the frame of the NCI approach, the 200 pm intermolecular distance corresponds to a large electronic density, out of the usual conditions of applications of NCI.[104] The interpretation of the system with a 250 pm intermolecular distance is tricky as the blue isosurface is still within the NCI regime; therefore it can be misleading. However, as can be seen in the 2D graph, another interaction is present. It is of repulsive nature (similar to the red crown around the interaction blue isosurface at 200 pm shown in Fig. 12a), and occurs at higher reduced density gradient values (typically in the 0.5–0.6 range). It is therefore beyond the scope of the NCI procedure and thus cannot be captured with the standard cut-off chosen for the 3D graphs (0.35) or even the 0.5 cut off chosen for Fig. 12. Of course, both interactions actually compete to stabilize the conformation and, despite the appearance of the sole blue pill, the repulsive interaction takes over leading to a destabilized conformation, with an overall positive interaction energy. In such cases, no conclusion about the global electronic energy should be drawn solely upon the 3D-NCI coloured isosurfaces, associated to low

density 2D-NCI troughs. Indeed, one should complement the interpretation by the incomplete (non-weak interactions anymore) repulsive troughs from the 2D graphs (see Fig. 12b). In any case, one should be cautious at very short distances as nuclear and Pauli repulsions dominate the weaker interactions at the energetic level.[104]

(3) Computational details

All computations have been performed at the B97-D/6-311++G** level (unless specified otherwise) using the Gaussian 09 package. All geometries have been fully optimized and do not present any imaginary frequency. All NCI computations have been performed using the NCI-Plot[63] package and use the densities obtained from the B97-D geometry optima.

Acknowledgements

The research described here has been supported by the French National Research Agency (ANR) (Grant ANR-08-BLAN-0158-01).

References

1 S. Steiner and G. R. Desiraju, *The Weak Hydrogen Bond*, Oxford University Press, Oxford, 1999.
2 S. Tsuzuki and A. Fujii, *Phys. Chem. Chem. Phys.*, 2008, **10**, 2584–2594.
3 M. P. D. Hatfield, N. Y. Palermo, J. Csontos, R. F. Murphy and S. Lovas, *J. Phys. Chem. B*, 2008, **112**, 3503–3508.
4 C. A. Schalley, *Mass Spectrom. Rev.*, 2001, **20**, 253–309.
5 R. Weinkauf, J. P. Schermann, M. S. de Vries and K. Kleinermanns, *Eur. Phys. J. D*, 2002, **20**, 309–316.
6 S. Maity, M. Guin, P. C. Singh and G. N. Patwari, *ChemPhysChem*, 2011, **12**, 26–46.
7 M. Honda, A. Fujii, E. Fujimaki, T. Ebata and N. Mikami, *J. Phys. Chem. A*, 2003, **107**, 3678–3686.
8 K. Yosida, K. Suzuki, S. Ishiuchi, M. Sakai, M. Fujii, C. E. H. Dessent and K. Müller-Dethlefs, *Phys. Chem. Chem. Phys.*, 2002, **4**, 2534–2538.
9 K. Sakota, N. Yamamoto, K. Ohashi, M. Saeki, S. Ishiuchi, M. Sakai, M. Fujii and H. Sekiya, *Chem. Phys.*, 2002, **283**, 209–219.
10 M. Mons, E. G. Robertson and J. P. Simons, *J. Phys. Chem. A*, 2000, **104**, 1430–1437.
11 K. Le Barbu, F. Lahmani, M. Mons, M. Broquier and A. Zehnacker, *Phys. Chem. Chem. Phys.*, 2001, **3**, 4684–4688.
12 K. Le Barbu-Debus, M. Broquier, F. Lahmani and A. Zehnacker-Rentien, *Mol. Phys.*, 2005, **103**, 1655–1662.
13 F. Lahmani, A. Zehnacker-Rentien and M. Broquier, *J. Photochem. Photobiol., A*, 2002, **154**, 41–52.
14 F. Lahmani, M. Broquier and A. Zehnacker-Rentien, *Chem. Phys. Lett.*, 2002, **354**, 337–348.
15 M. Broquier, F. Lahmani, A. Zehnacker-Rentien, V. Brenner, P. Millie and A. Peremans, *J. Phys. Chem. A*, 2001, **105**, 6841–6850.
16 E. G. Buchanan, W. H. James, A. Gutberlet, J. C. Dean, L. Guo, S. H. Gellman and T. S. Zwier, *Faraday Discuss.*, 2011, **150**, 209–226.
17 K. Schwing, C. Reyheller, A. Schaly, S. Kubik and M. Gerhards, *ChemPhysChem*, 2011, **12**, 1981–1988.
18 H. Fricke, K. Schwing, A. Gerlach, C. Unterberg and M. Gerhards, *Phys. Chem. Chem. Phys.*, 2010, **12**, 3511–3521.
19 H. S. Biswal, Y. Loquais, B. Tardivel, E. Gloaguen and M. Mons, *J. Am. Chem. Soc.*, 2011, **133**, 3931–3942.
20 E. Gloaguen, B. de Courcy, J. P. Piquemal, J. Pilmé, O. Parisel, R. Pollet, H. S. Biswal, F. Piuzzi, B. Tardivel, M. Broquier and M. Mons, *J. Am. Chem. Soc.*, 2010, **132**, 11860–11863.
21 E. Gloaguen, F. Pagliarulo, V. Brenner, W. Chin, F. Piuzzi, B. Tardivel and M. Mons, *Phys. Chem. Chem. Phys.*, 2007, **9**, 4491–4497.
22 V. Brenner, F. Piuzzi, I. Dimicoli, B. Tardivel and M. Mons, *Angew. Chem., Int. Ed.*, 2007, **46**, 2463–2466.
23 V. Brenner, F. Piuzzi, I. Dimicoli, B. Tardivel and M. Mons, *J. Phys. Chem. A*, 2007, **111**, 7347–7354.
24 W. Chin, F. Piuzzi, I. Dimicoli and M. Mons, *Phys. Chem. Chem. Phys.*, 2006, **8**, 1033–1048.
25 T. D. Vaden, S. A. N. Gowers, T. S. J. A. de Boer, J. D. Steill, J. Oomens and L. C. Snoek, *J. Am. Chem. Soc.*, 2008, **130**, 14640–14650.
26 J. A. Stearns, M. Guidi, O. V. Boyarkin and T. R. Rizzo, *J. Chem. Phys.*, 2007, **127**, 154322.
27 R. C. Dunbar, J. D. Steill and J. Oomens, *Int. J. Mass Spectrom.*, 2010, **297**, 107–115.
28 D. Semrouni, O. P. Balaj, F. Calvo, C. F. Correia, C. Clavaguera and G. Ohanessian, *J. Am. Soc. Mass Spectrom.*, 2010, **21**, 728–738.
29 P. Hobza, V. Spirko, Z. Havlas, K. Buchhold, B. Reimann, H. D. Barth and B. Brutschy, *Chem. Phys. Lett.*, 1999, **299**, 180–186.
30 B. C. Dian, A. Longarte, S. Mercier, D. A. Evans, D. J. Wales and T. S. Zwier, *J. Chem. Phys.*, 2002, **117**, 10688–10702.
31 B. C. Dian, A. Longarte and T. S. Zwier, *Science*, 2002, **296**, 2369–2373.
32 T. S. Zwier, *J. Phys. Chem. A*, 2006, **110**, 4133–4150.
33 W. H. James III, E. G. Buchanan, C. W. Mueller, J. C. Dean, D. Kosenkov, L. V. Slipchenko, L. Guo, A. G. Reidenbach, S. H. Gellman and T. S. Zwier, *J. Phys. Chem. A*, 2011, **115**, 13783–13798.
34 E. G. Buchanan, W. H. James, S. H. Choi, L. Guo, S. H. Gellman, C. W. Mueller and T. S. Zwier, *J. Chem. Phys.*, 2012, **137**, 094301.
35 A. Gerlach, C. Unterberg, H. Fricke and M. Gerhards, *Mol. Phys.*, 2005, **103**, 1521–1529.
36 H. Fricke, A. Gerlach and M. Gerhards, *Phys. Chem. Chem. Phys.*, 2006, **8**, 1660–1662.
37 W. Chin, F. Piuzzi, J. P. Dognon, I. Dimicoli and M. Mons, *J. Chem. Phys.*, 2005, **123**, 084301.
38 W. Chin, F. Piuzzi, J. P. Dognon, L. Dimicoli, B. Tardivel and M. Mons, *J. Am. Chem. Soc.*, 2005, **127**, 11900–11901.
39 Y. Loquais, E. Gloaguen, J. Thomas, M. Mons and D. W. Pratt, *J. Phys. Chem. B*, in press.

40 E. Gloaguen, Y. Loquais, J. A. Thomas, D. W. Pratt and M. Mons, *J. Phys. Chem. B*, 2013, **117**, 4945–4955.
41 T. Scharge, T. Haber and M. A. Suhm, *Phys. Chem. Chem. Phys.*, 2006, **8**, 4664–4667.
42 N. Seurre, K. Le Barbu-Debus, F. Lahmani, A. Zehnacker, N. Borho and M. A. Suhm, *Phys. Chem. Chem. Phys.*, 2006, **8**, 1007–1016.
43 N. Borho and Y. J. Xu, *Angew. Chem., Int. Ed.*, 2007, **46**, 2276–2279.
44 M. Albrecht, J. Will and M. A. Suhm, *Angew. Chem., Int. Ed.*, 2010, **49**, 6203–6206.
45 M. Speranza, F. Rondino, M. Satta, A. Paladini, A. Giardini, D. Catone and S. Piccirillo, *Chirality*, 2009, **21**, 119–144.
46 *Chiral Recognition in the Gas Phase*, ed. A. Zehnacker, CRC Press Taylor & Francis Group, Boca Raton, 2010.
47 R. Sudha and M. F. Jarrold, *J. Phys. Chem. B*, 2005, **109**, 11777–11780.
48 R. C. Dunbar, J. D. Steill and J. Oomens, *J. Am. Chem. Soc.*, 2011, **133**, 1212–1215.
49 K. Le Barbu, V. Brenner, P. Millie, F. Lahmani and A. Zehnacker-Rentien, *J. Phys. Chem. A*, 1998, **102**, 128–137.
50 M. Mons, F. Piuzzi, I. Dimicoli, A. Zehnacker and F. Lahmani, *Phys. Chem. Chem. Phys.*, 2000, **2**, 5065–5070.
51 N. Seurre, K. Le Barbu-Debus, F. Lahmani, A. Zehnacker-Rentien and J. Sepiol, *J. Mol. Struct.*, 2004, **692**, 127–137.
52 N. Seurre, J. Sepiol, K. Le Barbu-Debus, F. Lahmani and A. Zehnacker-Rentien, *Phys. Chem. Chem. Phys.*, 2004, **6**, 2867–2877.
53 M. Albrecht, A. Borba, K. Le Barbu-Debus, B. Dittrich, R. Fausto, S. Grimme, A. Mahjoub, M. Nedic, U. Schmitt, L. Schrader, M. A. Suhm, A. Zehnacker-Rentien and J. Zischang, *New J. Chem.*, 2010, **34**, 1266–1285.
54 D. Scuderi, K. Le Barbu-Debus and A. Zehnacker, *Phys. Chem. Chem. Phys.*, 2011, **13**, 17916–17929.
55 R. F. W. Bader, *Chem. Rev.*, 1991, **91**, 893–928.
56 S. Noury, X. Krokidis, F. Fuster and B. Silvi, *Comput. Chem.*, 1999, **23**, 597–604.
57 J. Poater, M. Duran, M. Sola and B. Silvi, *Chem. Rev.*, 2005, **105**, 3911–3947.
58 P. L. A. Popelier and G. Logothetis, *J. Organomet. Chem.*, 1998, **555**, 101–111.
59 P. L. A. Popelier, *Atoms in Molecules: An Introduction*, Prentice Hall PTR, 2000.
60 P. L. A. Popelier and R. F. W. Bader, *Chem. Phys. Lett.*, 1992, **189**, 542–548.
61 E. Espinosa, M. Souhassou, H. Lachekar and C. Lecomte, *Acta Crystallogr., Sect. B: Struct. Sci.*, 1999, **55**, 563–572.
62 (*a*) B. J. Miller, J. R. Lane and H. G. Kjaergaard, *Phys. Chem. Chem. Phys.*, 2011, **13**, 14183–14193; (*b*) J. R. Lane, J. Contreras-Garcia, J.-P. Piquemal, B. J. Miller and H. G. Kjaergaar, *J. Chem. Theory Comput.*, 2013, **9**, 3263–3266.
63 J. Contreras-Garcia, E. R. Johnson, S. Keinan, R. Chaudret, J. P. Piquemal, D. N. Beratan and W. T. Yang, *J. Chem. Theory Comput.*, 2011, **7**, 625–632.
64 E. R. Johnson, S. Keinan, P. Mori-Sanchez, J. Contreras-Garcia, A. J. Cohen and W. Yang, *J. Am. Chem. Soc.*, 2010, **132**, 6498–6506.
65 N. Gillet, R. Chaudret, J. Contreras-Garcia, W. T. Yang, B. Silvi and J. P. Piquemal, *J. Chem. Theory Comput.*, 2012, **8**, 3993–3997.
66 G. A. Chass, R. S. Mirasol, D. H. Setiadi, T. H. Tang, W. Chin, M. Mons, I. Dimicoli, J. P. Dognon, B. Viskolcz, S. Lovas, B. Penke and I. G. Csizmadia, *J. Phys. Chem. A*, 2005, **109**, 5289–5302.
67 W. Chin, M. Mons, J. P. Dognon, R. Mirasol, G. Chass, I. Dimicoli, F. Piuzzi, P. Butz, B. Tardivel, I. Compagnon, G. von Helden and G. Meijer, *J. Phys. Chem. A*, 2005, **109**, 5281–5288.
68 W. Chin, M. Mons, J. P. Dognon, F. Piuzzi, B. Tardivel and I. Dimicoli, *Phys. Chem. Chem. Phys.*, 2004, **6**, 2700–2709.
69 W. Chin, J. P. Dognon, F. Piuzzi, B. Tardivel, I. Dimicoli and M. Mons, *J. Am. Chem. Soc.*, 2005, **127**, 707–712.
70 W. Chin, J. P. Dognon, C. Canuel, F. Piuzzi, I. Dimicoli, M. Mons, I. Compagnon, G. von Helden and G. Meijer, *J. Chem. Phys.*, 2005, **122**, 054317.
71 C. F. P. Silva, M. L. T. S. Duarte and R. Fausto, *J. Mol. Struct.*, 1999, **482–483**, 591–599.
72 K. Le Barbu, F. Lahmani and A. Zehnacker-Rentien, *J. Phys. Chem. A*, 2002, **106**, 6271–6278.
73 A. Mahjoub, A. Chakraborty, V. Lepere, K. Le Barbu-Debus, N. Guchhait and A. Zehnacker, *Phys. Chem. Chem. Phys.*, 2009, **11**, 5160–5169.
74 E. E. Baquero, W. H. James, S. H. Choi, S. H. Gellman and T. S. Zwier, *J. Am. Chem. Soc.*, 2008, **130**, 4784–4794.
75 E. E. Baquero, W. H. James III, S. H. Choi, S. H. Gellman and T. S. Zwier, *J. Am. Chem. Soc.*, 2008, **130**, 4795–4807.
76 W. Chin, I. Compagnon, J. P. Dognon, C. Canuel, F. Piuzzi, I. Dimicoli, G. von Helden, G. Meijer and M. Mons, *J. Am. Chem. Soc.*, 2005, **127**, 1388–1389.
77 W. Chin, J. P. Dognon, F. Piuzzi, I. Dimicoli and M. Mons, *Mol. Phys.*, 2005, **103**, 1579–1587.
78 M. Gerhards, C. Unterberg, A. Gerlach and A. Jansen, *Phys. Chem. Chem. Phys.*, 2004, **6**, 2682–2690.
79 E. Gloaguen, R. Pollet, F. Piuzzi, B. Tardivel and M. Mons, *Phys. Chem. Chem. Phys.*, 2009, **11**, 11385–11388.
80 W. H. James, E. E. Baquero, S. H. Choi, S. H. Gellman and T. S. Zwier, *J. Phys. Chem. A*, 2010, **114**, 1581–1591.
81 W. H. James III, E. G. Buchanan, L. Guo, S. H. Geman and T. S. Zwier, *J. Phys. Chem. A*, 2011, **115**, 11960–11970.
82 E. Gloaguen, H. Valdes, F. Pagliarulo, R. Pollet, B. Tardivel, P. Hobza, F. o. Piuzzi and M. Mons, *J. Phys. Chem. A*, 2009, **114**, 2973–2982.
83 W. H. Pirkle and T. C. Pochapsky, *Chem. Rev.*, 1989, **89**, 347–362.
84 A. Zehnacker and M. A. Suhm, *Angew. Chem., Int. Ed.*, 2008, **47**, 6970–6992.
85 X. L. Kong, I. A. Tsai, S. Sabu, C. C. Han, Y. T. Lee, H. C. Chang, S. Y. Tu, A. H. Kung and C. C. Wu, *Angew. Chem., Int. Ed.*, 2006, **45**, 4130–4134.
86 J. L. Arbour, H. S. Rzepa, J. Contreras-Garcia, L. A. Adrio, E. M. Barreiro and K. K. Hii, *Chem.–Eur. J.*, 2012, **18**, 11317–11324.

87 A. Bouchet, T. Brotin, M. Linares, H. Agren, D. Cavagnat and T. Buffeteau, *J. Org. Chem.*, 2011, **76**, 4178–4181.
88 M. Nishijima, T. C. S. Pace, A. Nakamura, T. Mori, T. Wada, C. Bohne and Y. Inoue, *J. Org. Chem.*, 2007, **72**, 2707–2715.
89 T. B. Adler, N. Borho, M. Reiher and M. A. Suhm, *Angew. Chem., Int. Ed.*, 2006, **45**, 3440–3445.
90 N. Borho and M. A. Suhm, *Phys. Chem. Chem. Phys.*, 2004, **6**, 2885–2890.
91 Z. Su, N. Borho and Y. J. Xu, *J. Am. Chem. Soc.*, 2006, **128**, 17126–17131.
92 J. Thomas, F. X. Sunahori, N. Borho and Y. Xu, *Chem.–Eur. J.*, 2011, **17**, 4582–4587.
93 A. Latini, D. Toja, A. Giardini-Guidoni, S. Piccirillo and M. Speranza, *Angew. Chem., Int. Ed.*, 1999, **38**, 815–817.
94 A. Giardini-Guidoni, A. Paladini, F. Rondino, S. Piccirillo, M. Satta and M. Speranza, *Org. Biomol. Chem.*, 2005, **3**, 3984–3989.
95 K. Le Barbu-Debus, M. Broquier, A. Mahjoub and A. Zehnacker-Rentien, *J. Phys. Chem. A*, 2008, **112**, 9731–9741.
96 K. Le Barbu-Debus, F. Lahmani, A. Zehnacker-Rentien and N. Guchhait, *Chem. Phys. Lett.*, 2006, **422**, 218–225.
97 K. Le Barbu-Debus, M. Broquier, A. Mahjoub and A. Zehnacker-Rentien, *Phys. Chem. Chem. Phys.*, 2009, **11**, 7589–7598.
98 S. Tsuzuki, K. Honda, A. Fujii, T. Uchimaru and M. Mikami, *Phys. Chem. Chem. Phys.*, 2008, **10**, 2860–2865.
99 A. Savin, B. Silvi and F. Colonna, *Can. J. Chem.*, 1996, **74**, 1088–1096.
100 B. Silvi, *J. Mol. Struct.*, 2002, **614**, 3–10.
101 B. Silvi and A. Savin, *Nature*, 1994, **371**, 683–686.
102 D. Fang, R. Chaudret, J. P. Piquemal and G. A. Cisneros, *J. Chem. Theory Comput.*, 2013, **9**, 2156–2160.
103 F. R. Wagner, V. Bezugly, M. Kohout and Y. Grin, *Chem.–Eur. J.*, 2007, **13**, 5724–5741.
104 J. Contreras-Garcia, W. T. Yang and E. R. Johnson, *J. Phys. Chem. A*, 2011, **115**, 12983–12990.